arXiv:1512.09004v5 [cond-mat.mes-hall] 28 Mar 2016

Thermal smearing of the magneto-Kohn anomaly for Dirac materials and comparison with the two-dimensional electron liquid

Godfrey Gumbs[1,2], Antonios Balassis[3], Dipendra Dahal[1], M. L. Glasser[2,4]

[1]*Department of Physics,*

Hunter College of City University of New York,

695 Park Avenue,

New York, NY 10065, USA

[2]*Donostia International Physics Center,*

P. Manuel de Lardizabal 4,

20018 San Sebastian, Spain

[3]*Department of Physics,*

Fordham University,

Bronx, NY 10458, USA

[4]*Department of Physics,*

Clarkson University, Potsdam,

New York 13699-5820, USA

(Dated: March 29, 2016)

Abstract

We compute and compare the effects due to a uniform perpendicular magnetic field as well as temperature on the static polarization functions for monolayer graphene (MLG), associated with the Dirac point, with that for the two-dimensional electron liquid (2DEL) with the use of comprehensive numerical calculations. The relevance of our study to the Kohn anomaly in low-dimensional structures and the Friedel oscillations for the screening of the potential for a dilute distribution of impurities is reported. Our results show substantial differences due to screening for the 2DEL and MLG which have not been given adequate attention previously.

PACS numbers: 73.21.-b, 71.10.-w, 73.43.Lp, 24.10.Cn, 68.65.Pq

I. INTRODUCTION

There have been recent experimental reports regarding the observation that there is direct evidence of the role played by screening of charged impurities in graphene and the two-dimensional electron liquid on their properties [1, 2]. Specifically, it has been demonstrated that in the presence of a magnetic field the strength of the impurity scattering can be adjusted by controlling the occupation of Landau-level states, which enters the polarizability. The presence of impurities may produce potential fluctuations whose amplitude can depend on both the density of ions, their location, magnetic field and temperature which can affect their high mobility. These considerations are relevant in the design and efficiency of semiconductor field effect transistors. An interesting paper in Ref. [3] investigating the smearing of the Kohn anomaly for a two-dimensional electron liquid (2DEL) in a perpendicular weak magnetic field was published a few years ago. There, the principal goal was obtaining a closed-form analytic expression for the Landau level contribution to the random-phase approximation (RPA) static polarization operator $\Pi(q, \omega = 0)$, where q denotes the wave vector transfer. Also, at that time, a simple exact expression for $\Pi(q, \omega)$ valid for all temperatures, frequencies ω and non-quantizing magnetic fields [4] existed in the literature (see also Refs. [5, 6]) and taking its derivative with respect to wave number may be carried out in a straightforward way.

In this paper we intend to examine the behavior of the static polarizability and shielded potential in the strong field limit for monolayer graphene and the 2DEL by carrying out detailed numerical calculations. To bolster confidence in our numerical procedure, we compare our data obtained with that already reported in the literature for special cases, as we have pointed out below.

We investigate the smearing of the Kohn anomaly in graphene [7–18] and the 2DEL [7, 8, 19] by numerically calculating the static polarization function along with its derivative for various magnetic field strengths and temperatures. We also report results for the screening of an impurity embedded within or near a 2DEL and a graphene layer. Our results at zero-temperature are in general agreement with those presented in Ref. [8].

The outline of the rest of our presentation is as follows. In Sec. II, we detail the Hamiltonian we employ for the Dirac electrons in MLG under the influence of a perpendicular

ambient magnetic field as well as the 2D RPA ring diagram polarization function for graphene at finite temperature. A careful calculation of the polarization function for a range of temperature and magnetic field is reported in Sec. III along with the associated screening of impurities. We demonstrate that the analytic features in the polarization function are directly reflected in those obtained for static shielding and so are detectable experimentally. We conclude with highlights of our calculations in Sec. IV.

II. MODEL FOR GRAPHENE LAYER AND THE POLARIZATION FUNCTION IN MAGNETIC FIELD

Let us consider electrons in a single graphene layer in the $x-y$ plane in a perpendicular magnetic field $\mathbf{B}$ parallel to the positive z axis. The effective-mass Hamiltonian for noninteracting electrons in one valley in graphene in the absence of scatterers is given by the following equation. Here, we neglect the Zeeman splitting and assume valley-energy degeneracy, describing the eigenstates by two pseudospins. We have,

$$\hat{H}_0 = v_F \begin{pmatrix} 0 & \hat{\pi}_x - i\hat{\pi}_y \\ \hat{\pi}_x + i\hat{\pi}_y & 0 \end{pmatrix} , \tag{1}$$

where $\hat{\pi} = -i\hbar\nabla + e\mathbf{A}$, $-e$ is the electron charge, $\mathbf{A}$ is the vector potential, $v_F = \sqrt{3}at/(2\hbar)$ is the Fermi velocity with $a = 2.57$ Å denoting the lattice constant and $t \approx 2.71$ eV is the overlap integral between nearest-neighbor carbon atoms.

In the Landau gauge $\mathbf{A} = (0, Bx, 0)$, the eigenfunctions $\psi_\alpha(\mathbf{r})$ of the Hamiltonian $\hat{H}_0$ in Eq. (1) are labeled by the set of quantum numbers $\alpha = \{k_y, n, s(n)\}$ where $n = 0, 1, 2, \cdots$ is the Landau level index, k_y is the electron wave vector in the y direction, and $s(n)$ defined by $s(n) = 0$ for $n = 0$ and $s(n) = \pm 1$ for $n > 0$ indicates the conduction $(+1)$ and valence $(-1$ and $0)$ bands, respectively. The two-component eigenfunction $\psi_\alpha(\mathbf{r})$ is given by

$$\psi_\alpha(x, y) = \frac{C_n}{\sqrt{L_y}} e^{ik_y y} \begin{pmatrix} s(n) i^{n-1} \Phi_{n-1}(x + l_B^2 k_y) \\ i^n \Phi_n(x + l_B^2 k_y) \end{pmatrix} , \tag{2}$$

where $l_B = \sqrt{\hbar/eB}$ is the magnetic length, and L_x and L_y are normalization lengths in the x and y directions. Also, $A = L_x L_y$ is the area of the system. We have $C_n = 1$ for $n = 0$

and $1/\sqrt{2}$ for $n > 0$. Additionally, we have

$$\Phi_n(x) = \left(2^n n! \sqrt{\pi} l_B\right)^{-1/2} \exp\left[-\frac{1}{2}\left(\frac{x}{l_B}\right)^2\right] H_n\left(\frac{x}{l_B}\right) \ , \tag{3}$$

where $H_n(x)$ is a Hermite polynomial. The eigenenergies depend on the quantum numbers n and s only and are given by

$$\epsilon_{ns} = s(n)\epsilon_n = s(n)\frac{\hbar v_F}{l_B}\sqrt{2n} \ . \tag{4}$$

Note that the ratio of the Zeeman term $\Delta E_Z(B)$ to the separation between adjacent Landau levels $\Delta E_L(B)$ is negligible at high magnetic field. For $B = 10$ T, we have $\Delta E_Z(B)/\Delta E_L(B) \approx \mu_B B/(\sqrt{2}\hbar v_F l_B^{-1}) \approx 5 \times 10^{-3}$. Here, $\mu_B = e\hbar/(2m_e)$ is the Bohr magneton with m_e denoting the free electron mass. Therefore, the contributions to the single-electron Hamiltonian from the Zeeman splitting and very small pseudospin splitting caused by two valleys in graphene may be neglected. We assume energy degeneracy for the two possible spin projections and two graphene valleys described by pseudospins.

The 2D polarization function is given by [7–9]

$$\Pi(q,\omega) = \frac{g}{2\pi l_B^2}\sum_{n=0}^{\infty}\sum_{n'=0}^{\infty}\sum_{s,s'=\pm}\frac{f_0(\epsilon_{ns}) - f_0(\epsilon_{n's'})}{\epsilon_{ns} - \epsilon_{n's'} + \hbar\omega + i\delta}F_{nn'}^{ss'}(q) \ , \tag{5}$$

where, $g = 4$ for the spin and valley degeneracy, $f_0(\epsilon_{ns}) = 1/\left[e^{(\epsilon_{ns}-\mu)/k_BT} + 1\right]$ is the Fermi distribution function,with s,$s' = \pm 1$, $\epsilon_{ns} = (s\hbar v_F/l_B)\sqrt{2n} - E_F$, where E_F is the Fermi energy and the form factor $F_{nn'}^{ss'}(q)$ is defined as

$$\begin{aligned} F_{nn'}^{ss'}(q) \ &= \ e^{-l_B^2q^2/2}\left(\frac{l_B^2q^2}{2}\right)^{(n_>-n_<)} \\ &\times \ \left(s1_n^*1_{n'}^*\sqrt{\frac{(n_<-1)!}{(n_>-1)!}}L_{n_<-1}^{n_>-n_<}(l_B^2q^2/2) + s'2_n^*2_{n'}^*\sqrt{\frac{n_<!}{n_>!}}L_{n_<}^{n_>-n_<}(l_B^2q^2/2)\right)^2 \end{aligned} \tag{6}$$

Here, $1_n^* = [(1-\delta_{n,0})/2]^{1/2}$, $2_n^* = [(1+\delta_{n,0})/2]^{1/2}$, $n_>$=max(n,n'), $n_<$=min(n,n') and $L_n^a(x)$ is the associated Laguerre polynomial. At $T = 0$ K we have,

$$\Pi_{\rm inter}(q,\omega) = \sum_{n=0}^{N_c}\sum_{n'=N_F}^{N_c}\frac{F_{nn'}^{-+}}{-\epsilon_n - \epsilon_{n'} + \hbar\omega + i\delta} + (\hbar\omega_+ \to \hbar\omega_-) \tag{7}$$

with, N_F being the filling factor, $\hbar\omega_\pm = \pm(\hbar\omega + i\delta)$, $s = -1$ and $s' = +1$. We also have

$$\Pi_{\rm intra}(q,\omega) = \sum_{n=0}^{N_F-1}\sum_{n'=N_F}^{N_c}\frac{F_{nn'}^{++}}{\epsilon_n - \epsilon_{n'} + \hbar\omega + i\delta} + (\hbar\omega_+ \to \hbar\omega_-) \tag{8}$$

and the total polarizability is obtained from

$$\Pi(q,\omega) = \Pi_{\rm inter}(q,\omega) + \Pi_{\rm intra}(q,\omega) \ , \tag{9}$$

where $\Pi_{\rm inter}(q,\omega)$ is due to transitions from the valence to the conduction band while $\Pi_{\rm intra}(q,\omega)$ accounts for transitions within the conduction band. We must also note that the chemical potential depends on temperature approximately as

$$\mu \approx E_F \left\{ 1 - \frac{\pi^2}{6} \frac{d\ln(\rho(E_F))}{d\ln(E_F)} \left(\frac{k_B T}{E_F} \right)^2 + \cdots \right\} \tag{10}$$

where $\rho(E_F)$ is the density-of-states at the Fermi energy E_F. Of course, for graphene, we have $\rho(\epsilon) = \epsilon/[\pi(\hbar v_F)^2]$ whereas for the 2DEL the density of states is constant and given by $\rho(\epsilon) = m^*/\pi\hbar^2$ so that we can replace the chemical potential by the Fermi energy when the temperature of the 2DEL is low. Furthermore, in calculating the temperature-dependence of the polarization function at low temperature ($k_B T \ll E_F$), we employ $f_0(\epsilon;T) \approx \theta(E_F - \epsilon) - (k_B T)\delta(\epsilon - E_F)$ in terms of the Heaviside step-function $\theta(x)$.

In evaluating the finite-temperature polarization, we may employ the following transformation of Maldague [6] relating its values in the absence ($T = 0$) and presence of a heat bath in the absence of magnetic field, i.e.,

$$\Pi(q,\omega;T) = \int_0^\infty d\,E \frac{\Pi_{T=0,E_F=E}(q,\omega)}{4k_B T \cosh^2\left[\frac{E-\mu(T)}{2k_B T}\right]} \ . \tag{11}$$

Recently, a generalization of this transformation to graphene when an external magnetic field is applied was given in [17]. At high temperatures or weak magnetic field, when the separation between Landau levels is small, and $k_B T \gg \hbar v_F/l_B$, the occupation of the Landau levels is given by the Fermi-Dirac distribution function $f_{n,s(n)} = 1/\left[e^{\left(\epsilon_{n,s(n)}/k_B T\right)} + 1\right]$ for $n > 0$ if the energy is measured from the Fermi level. When the magnetic field is sufficiently high, Landau level separation is large and we may take only a few terms in the polarization sums since transitions to higher levels have smaller oscillator strengths. Furthermore, the separation between Landau levels decreases as n increases and is $\propto 1/\sqrt{n}$, for large n. In our calculations, we included Landau levels with $1 < n \leq 70$ unless stated otherwise. We may separate the contributions to the polarization $\Pi(q,\omega)$ into contributions which correspond to transitions between different Landau levels inside the conduction band, and this term does not contribute at $T = 0$ K.

We may now make use of our result for the polarization function to calculate the shielded potential of a point charge on the polar axis at a distance z_0 from the 2D plane. This is given as a Hankel transform of order zero by [20]

$$V\left(r_{\parallel}, z_0\right) = \left(\frac{e^2}{\epsilon_s}\right) \int_0^{\infty} dq \;\; J_0(qr_{\parallel}) e^{-qz_0} \frac{1}{\epsilon(q, \omega = 0)} \tag{12}$$

where the dielectric function is obtained in the random-phase-approximation (RPA) from

$$\epsilon(q, \omega) = 1 - \frac{2\pi e^2}{\epsilon_s q} \Pi\left(q, \omega\right) \tag{13}$$

and $\epsilon_s = 4\pi\varepsilon_0\epsilon_b$ with ε_0 the permeability of free space and ϵ_b the background dielectric constant. As a matter of fact, Eq. (12) determines the static density distribution around an impurity, as well as the effective interaction between two test charges embedded within the 2D structure. In general, the screened potential decreases exponentially with z_0 and is not of interest to us.

III. NUMERICAL RESULTS AND DISCUSSION

In our numerical calculations, we chose $r_s = 3.0$ for the 2DEL where we define $r_s = 2m^*e^2/(\epsilon_b k_F \hbar^2)$ in terms of the electron effective mass m^*, the background dielectric constant ϵ_b and the Fermi wave vector k_F. We chose $m^* = 0.067\ m_e$ (m_e is the free electron mass) and $\epsilon_b = 13.6$ which are appropriate for GaAs/AlGaAs. Then r_s corresponds to electron density $n = 6.1 \times 10^{10}$ cm^{-2}. For monolayer graphene, we chose $r_s = 1.0$ where now we define r_s by $r_s = e^2/(\epsilon_b \hbar v_F)$ given in terms of the Fermi velocity v_F for pristine graphene and the background dielectric constant for this material.

In Fig. 1, we present results from our calculations for the static polarization function $\Pi(q, \omega = 0)$ and the shielded potential for a 2DEL in the presence of a perpendicular magnetic field for two filling factors N_F at chosen temperatures. At $T = 0$ K, the polarization function has N_F sharp local maxima corresponding to the number of completely full Landau levels. As the temperature is increased, these peaks become smeared out and the polarizability is diminished. Correspondingly, the screened potential exhibits exactly the same number of local maxima as its polarization at $T = 0$ K responsible for dielectric screening. Just like the polarizability, there is smearing of these peaks when the temperature is increased [17]. We have $N_F = \pi l_B^2 n_{2D}$ at $T = 0$ K in terms of the electron density n_{2D}. The Fermi

wave vector k_F is also given by $k_F l_B = \sqrt{2N_F - 1}$. At $T = 0$ K, when there are multiple peaks, these peaks increase in height with increasing wave vector [19]. But, at finite temperature, the height of the peaks decreases with increasing wave vector. Irrespective of what temperature chosen, the first peak in the static polarizability function appears at $q \approx 2k_F$.

In Fig. 2, we have presented results for the polarization function and its derivative for a 2DEL for several filling factors ($N_F = 1, 2, 3, 4$) at $T = 0$ K. Additionally, in Fig. 3, we have demonstrated what effect temperature has on the derivative of polarization in Fig. 2 for the two cases when $N_F = 1, 2$. These results should be compared with those in Ref. [3] which show that the part of the curve for the derivative of the polarizability which connects the first local maximum with the first local minimum is a manifestation of the smoothing of the Fermi surface by temperature.

In the absence of any magnetic field, we may obtain the polarizability at $T = 0$ K by making use of the analytical formula of Stern [21]. In this case, the derivative function has a discontinuity at $2k_F$, i.e., twice the Fermi wave vector. In fact, between $0 < q < 2k_F$, the polarizability is constant and for $q > 2k_F$, it falls off like $1/q$. Although the polarizability function itself is continuous at $2k_F$, the abrupt change in slope is what gives the discontinuity in its derivative. The plots in Fig. 4 show that when we introduce temperature, there is an effect on the polarization function and subsequently on the screened potential. In accordance with our results above, we obtain a finite number of oscillatory peaks for a finite magnetic field which is increased as the magnetic field is reduced. Therefore, we have, as expected, the Friedel oscillations at $B = 0$ in Fig. 4 and whose amplitudes decrease with temperature.

At this point, we note that when we introduce magnetic field into the calculations, some distinct features arise. First, each of the plots in Figs. 1 through 3 for $\Pi^{(0)}(q, \omega = 0)$ for the 2DEL is dependent on wavevector in the long wavelength limit. However the polarization is constant over a wide range ($0 \leq q \leq 2k_F$) in the absence of magnetic field. The length scales in our plots for zero and finite magnetic field are related through the equation $k_F l_B = \sqrt{2N_F - 1}$. In the shorter wavelengths limit, the $1/q$ dependence now has oscillations, which is due to the presence of Laguerre polynomials in the form factor. Our conclusion from these calculations is that the number of peaks in the polarization function and its derivative is equal to the filling factor N_F for the number of filled Landau levels. This is also the same as the number of local maxima in the screened potential in the presence of magnetic field.

Turning now to the effect of temperature and magnetic field on *doped* monolayer graphene, we present plots in Fig. 5 for the static polarizability and the screened potential at various temperatures in the absence of an external magnetic field. In our numerical simulations, we employ an appropriate value for the Wigner-Seitz radius defined as the ratio of the potential to the kinetic energy in an interacting Coulomb system [12]. For comparison and explanation of the characteristic features we have obtained, we refer to the results previously obtained for the static polarization when $T = 0$ K and $B = 0$ [22] and for finite temperature in the absence of magnetic field [23]. The effect due to temperature between $0 < q < 2k_F$ is just as significant for doped graphene as for 2DEL since the constant polarization function in this range is independent on q at $T = 0$ K but is definitely wave vector dependent when the sample is heated. Our results in Fig. 5 for the screened potential show that there may be Friedel oscillations which become smeared with temperature and also when the charged impurity is moved away from the 2D layer of graphene. However, the major difference between the Friedel oscillations for the 2DEL and monolayer graphene is that in the former case, there are plus-to-minus oscillations as the distance from the impurity is increased. However, for monolayer graphene, the screened potential is always repulsive. This, of course, may directly be attributed to the difference in band structure for the two media and will indicate the difference in the many-body effects due to dielectric shielding.

Figure 6 shows our results for the static polarization function for monolayer graphene at $T = 0$ K when there is a magnetic field present. We present results corresponding to the cases when there are $N_F = 2, 3$ Landau levels filled. For clarity, we separated the contributions to the polarizability corresponding to intra-band and inter-band transitions. The intra-band static polarization function has the same number of peaks as the total number of occupied Landau levels, as is the case for the 2DEL where only conducting electrons are considered for transitions from below to above the Fermi level. For the inter-band polarization function, there is no restriction on the number of allowed transitions. Consequently, this is devoid of the "signature" peaks as its intra-band counterpart possesses. Adding these two parts leads us to our presented results which agree with those given by Roldan, et al. [8]. We emphasize that the Dirac cone approximation (in zero magnetic field) is valid only for a limited range range of energy ($0< \epsilon <300$ meV), thereby requiring that in carrying out our calculations, we must introduce a cut-off value N_c for the number of Landau levels in the presence of a uniform perpendicular magnetic field. Specifically, in Fig. 6, we chose the cut-off value

$N_c = 350$.

Our results above show that for 2DEL, there are N_F peaks in the polarization function as well as N_F peaks for the screened potential for chosen magnetic field. For graphene, there are also N_F peaks in the polarization function, coming from the N_F filled Landau levels, as we noted above. However, as we show in Fig. 7, there are N_F peaks in the screened potential which are clearly visible but these are very sensitive to whether or not the impurity is embedded within the 2D layer. When we set the impurity at a finite distance from the graphene layer, the peaks in the screened potential are smeared out. The sensitive nature of these results establishes a dramatic difference between MLG and the 2DEL.

The results here not only provide additional insight into the behavior of the static polarization function in strong magnetic fields over a range of temperature, but they demonstrate the many-body effects on the screening properties under these varying environmental conditions. Although the emphasis has been on integer filling of the Landau levels, we may extend our calculations to the case when there is fractional filling. Our calculations show that substantial differences occur between the 2DEL and monolayer graphene in the $q \to 0$ limit where the filling factor response functions have different functional dependences on the wave vector due to the absence of low-energy excitations when $B \neq 0$, contrary to the contribution from the energy bands to the Lindhard function in the absence of magnetic field. From a mathematical point of view, this difference is due to the sum over n, n'-sum being dominated by the $n_> - n_< = 1$ term in Eq. (5), i.e., by the highest occupied and the lowest unoccupied Landau level. Figures 1 through 3 show oscillations for finite filling factor, for intermediate wave vector. However, these oscillations in $\Pi(q, 0)$ subside with increasing N_F in accordance with Fig. 4, and the screened potential exhibits the Friedel-like oscillations as a function of displacement. Similar conclusions are obtained for monolayer graphene, as we have shown.

IV. CONCLUDING REMARKS AND SUMMARY

We have presented a comprehensive description of the combined effect of temperature and magnetic field on the static polarization function for MLG associated with the Dirac point. For completeness, we calculated numerically the polarizability for the 2DEL under a uniform perpendicular magnetic field at finite temperature. Our results for the 2DEL are

concerned with the effect due to a strong magnetic field on the polarizability and screening in monolayer graphene and the 2DEL. This is in contrast with Ref. 3 where the weak field limit was emphasized. The results we obtained are given in an experimentally achievable long wavelength regime. Besides, the numerical results were obtained at low temperature where the sharpness of the Fermi surface is evident and at high enough temperature which brought to bear the effect which heating may have on this property of the electron liquid.

Among our main conclusions which arise from our calculations in this paper, we have obtained the following. For doped MLG, the most important effect occurs in the limit $q \to 0$ for any filling factor N_F and any temperature, as well as at larger wave vectors (beyond $q > 2k_F$) when the temperature is high. At $T = 0$ K, it is clear from a mathematical point of view that the polarizability is dominated by transitions from the highest occupied to the lowest unoccupied Landau level. As the temperature is increased, other transitions contribute thereby leading to a smearing of the low-temperature structure. If the magnetic field is sufficiently high, then the Landau level separation is large. Consequently, we may take only a few terms in the polarization sums since transitions to higher levels have smaller oscillator strengths.

---

[1] T. Ferrus, R. George, C. H. W. Barnes and M. Pepper Appl. Phys. Lett. **97**, 142108 (2010).

[2] Adina Luican-Mayer, Maxim Kharitonov, Guohong Li, Chih-Pin Lu, Ivan Skachko, Alem-Mar B. Goncalves, K. Watanabe, T. Taniguchi, and Eva Y. Andrei, Phys. Rev. Lett. **112**, 036804 (2014).

[3] T. A. Sedrakyan, E. G. Mishchenko, and M. E. Raikh, Phys. Rev. Lett. **99**, 036401 (2007).

[4] M. L. Glasser, Phys. Rev. B **28**, 4387 (1983).

[5] I. L. Aleiner and L. I Glazman, Phys. Rev. B **52**, 11296 (1995).

[6] P. F. Maldague, Surf. Sci. **73**, 296 (1978).

[7] R. Roldan, J.-N. Fuchs, and M. O. Goerbig, Phys. Rev. B **80**, 085408 (2009).

[8] R. Roldan, M. O. Goerbig and J.-N. Fuchs, Semicond. Sci. Technol. **25**, 034005 (2010).

[9] O. L. Berman, G. Gumbs, and Y. E. Lozovik, Phys. Rev. B **78**, 085401 (2008).

[10] S. Piscanec, M. Lazzeri, F. Mauri, A. C. Ferrari, and J. Robertson, Phys. Rev. Lett., **93**, 185503 (2004).

[11] D. L. Mafra, L. M. Malard, S. K. Doorn, Han Htoon, J. Nilsson, A. H. Castro Neto, and M. A. Pimenta, Phys. Rev. B **80**, 241414(R) (2009).

[12] E. H. Hwang and S. Das Sarma Phys. Rev. B **75**, 205418 (2007).

[13] E. H. Hwang and S. Das Sarma, Phys. Rev. Lett. **101**, 156802 (2008).

[14] S. Das Sarma and Q. Li, Phys. Rev. B **87**, 235418 (2013).

[15] T. Ando, Journal of the Physical Society of Japan Vol. 75, No. 7, July, 074716 (2006).

[16] B. Yan, L. Kong, and J. Lv, Plasma Science and Technology, **11**, (2009).

[17] P. K. Pyatkovskiy and V. P. Gusynin, Phys. Rev. B **83**, 075422 (2011).

[18] M. van Schilfgaarde and M. I. Katsnelson, Phys. Rev. B **83**, 081409(R) (2011).

[19] G. Giuliani and G. Vignale, *Quantum Theory of the Electron Liquid* (Cambridge University Press, 2008) p. 580.

[20] P. B. Visscher and L. M. Falicov, Phys. Rev. B **3**, 2541 (1971).

[21] F. Stern, Phys. Rev. Lett. **18**, 546 (1967).

[22] B. Wunsch, T. Stauber, F. Sols, and F. Guinea, New Journal of Phys. **8**, 318 (2006).

[23] E. H. Hwang and S. Das Sarma, Phys. Rev. B **79**, 165404 (2009).

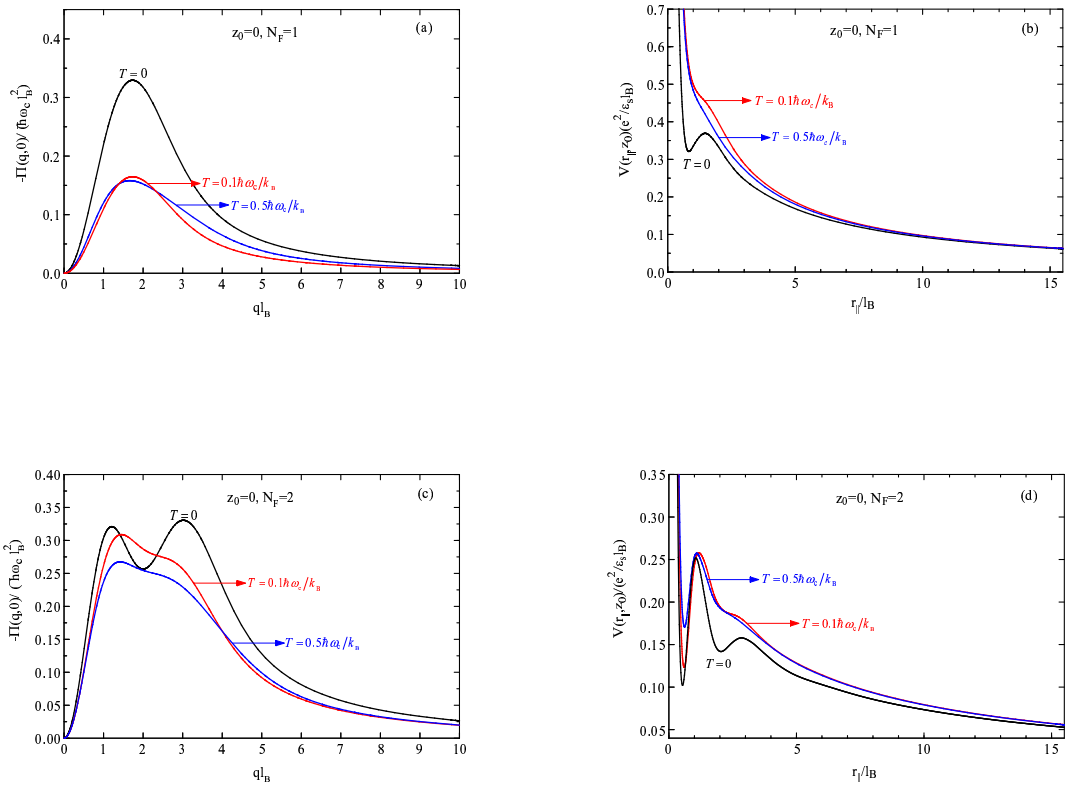

FIG. 1: (Color online) For two filling factors $N_F = 1, 2$, the static polarization function (left panels) for the 2DEL for various temperatures as a function of the wave vector q in units of the inverse magnetic length l_B^{-1}. The right panels show the corresponding screened potentials.

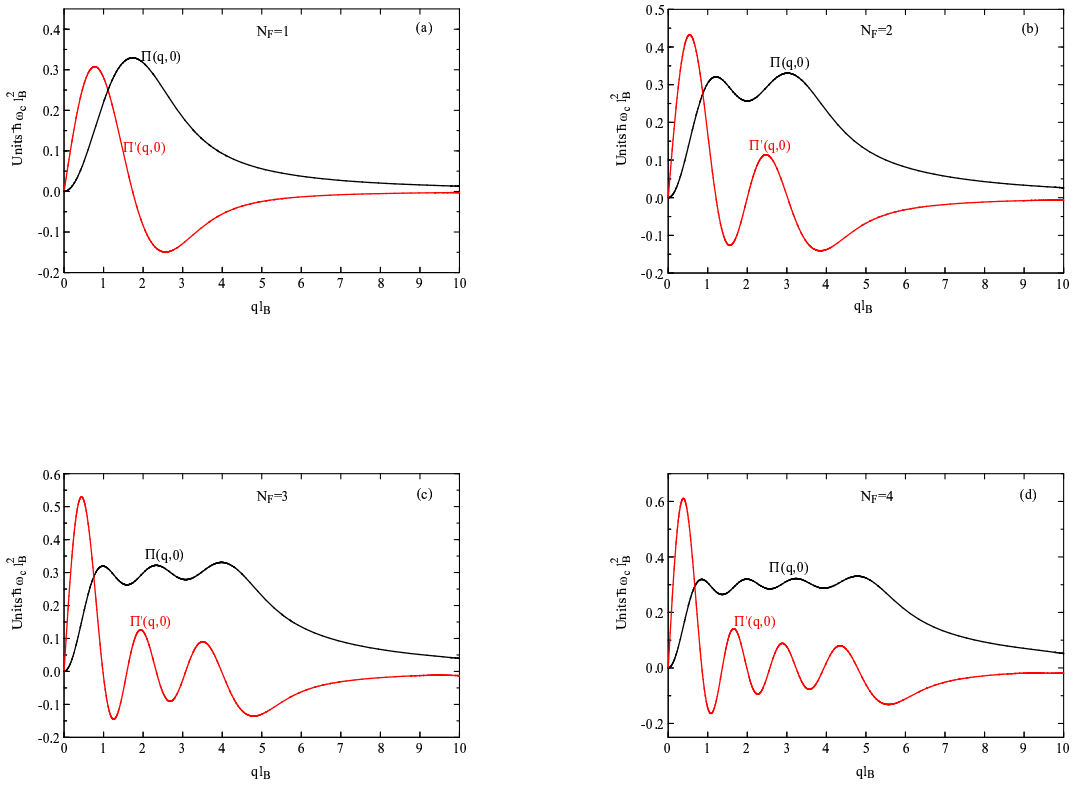

FIG. 2: (Color online) Static polarization function and its derivative for the 2DEL at $T = 0$ for various filling factors as a function of the wave vector q in units of the inverse magnetic length l_B^{-1}.

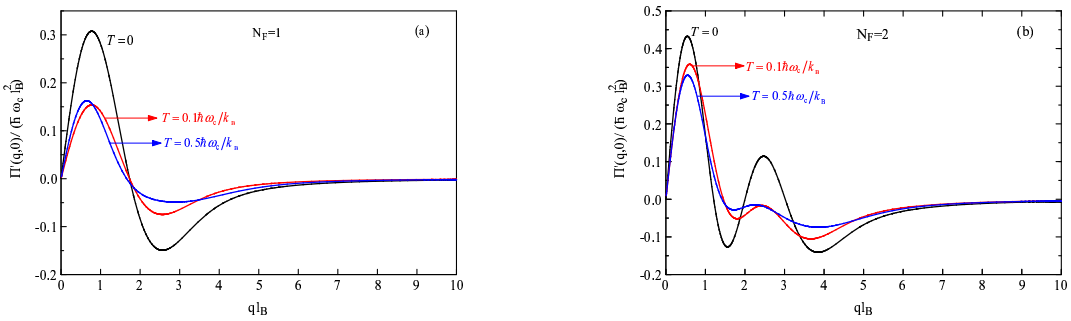

FIG. 3: (Color online) Derivative of the static polarization function for the 2DEL at various temperatures and a chosen filling factor as a function of the wave vector q in units of the inverse magnetic length l_B^{-1}.

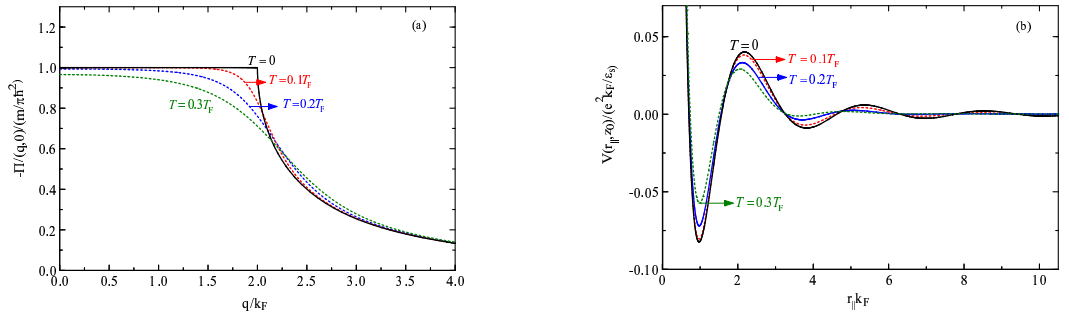

FIG. 4: (Color online) For various temperatures, the static polarization function (left panel) for the 2DEL at finite temperature in the absence of magnetic field as a function of the wave vector q in units of k_F. The right panel shows the corresponding screened potentials.

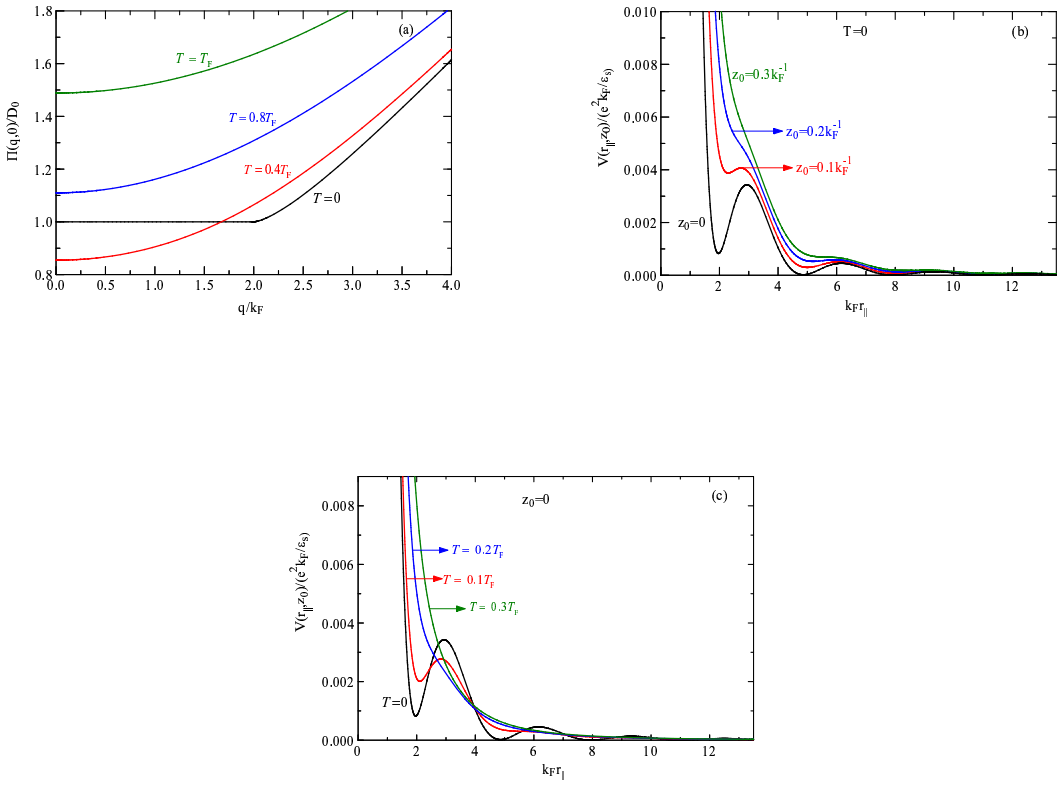

FIG. 5: (Color online) For Wigner-Seitz-Seitz radius $r_s = 1.0$ defined as $r_s = (e^2/\epsilon_b \hbar v_F)$, the static polarization function in (a) is plotted in units of the density-of-states at the Fermi level $D_0 = \rho(\epsilon_F)$ for MLG at $T = 0$ as well as finite temperature in the absence of magnetic field as a function of the wave vector q in units of k_F. The panels (b) and (c) show the corresponding screened potentials.

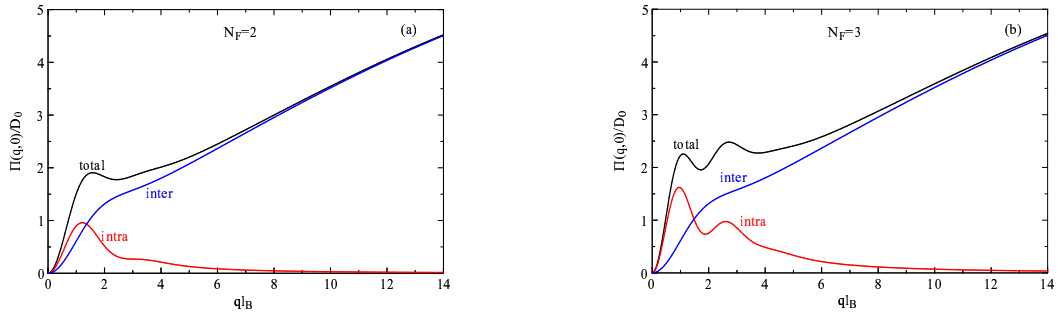

FIG. 6: (Color online) Static polarization function for MLG at $T = 0$ K in the presence of magnetic field as a function of the wave vector q in units of l_B^{-1}. The number of filled Landau levels was chosen as (a) $N_F = 2$ and (b) $N_F = 3$. The intra and inter-subband contributions are presented. The inset in (b) is for a larger range of wave vector and demonstrates that the polarizability eventually tends to zero in the short wavelength limit.

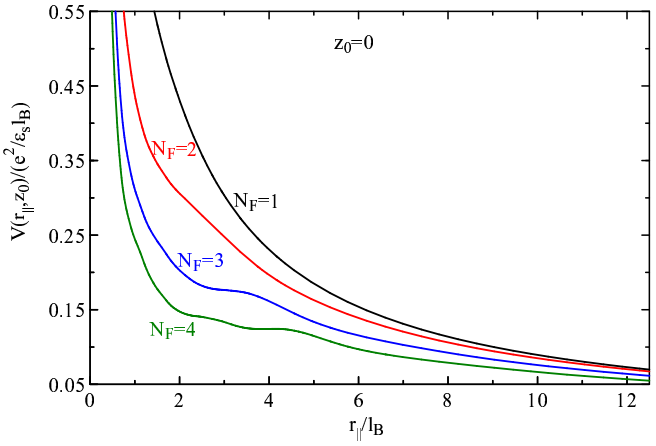

FIG. 7: (Color online) The screened potential for monolayer graphene at $T = 0$ K in the presence of magnetic field for various N_F. The results were obtained for chosen $z_0 = 0$, i.e., for an impurity imbedded within the 2D layer.